## SUPPLEMENTARY GEOLOGICAL SETTING AND PETROGRAPHY

The Orlica-Śnieżnik Dome (Fig. DR1A) is located on the north-eastern part of the Bohemian Massif. It consists of amphibolitic-grade orthogneisses with high and ultra-high pressure rocks inliers and subordinate staurolite grade supracrustal series (Don et al., 1990). Intrusion of the granitic precursor of the Orlica-Śnieżnik gneisses took place c. 520 – 490 Ma, (Oliver et al., 1993; Kröner et al., 2001; Štípská et al., 2004). Subsequently the whole complex underwent high grade metamorphism during Variscan orogeny at c. 350 – 330 Ma (Turniak et al., 2000; Lange et al., 2005; Gordon et al., 2005; Bröcker et al., 2009).
Within the Orlica-Śnieżnik gneisses (Fig. DR1A), high and ultra-high pressure rocks are represented by numerous eclogite bodies and one large body of felsic granulites with mafic granulite inliers. Samples of this granulitic body have been investigated in this study, after being collected in the most well-known and best-preserved in situ exposure in the area - in Stary Gierałtów, at the Biała Lądecka River bank (N50$^{o}$18,509`, E 016$^{o}$56,032`).

In the samples, garnet (<2mm in size) amounts to the 30-40% in modal amount of the rock, scattered in a leucocratic matrix (Fig. DR1B) of quartz, plagioclase and perthitic feldspar. Garnet contains kyanite, mesoperthite, quartz and rare clinopyroxene as mineral inclusions besides nanogranites. Titanite and rutile+titanite locally grow on garnet boundaries during the decompressional history of the rock (Carswell and O'Brien, 1993). No coesite or microstructures indicating its former presence were identified in the samples investigated for this study, despite quartz pseudomorphs after coesite has been reported in the area (Bakun-Czubarow, 1991).
Garnet is rich in almandine and grossular component, with a weak zoning characterized by a slight decrease in Alm and Grs toward the rim balanced by Prp increase (mineral chemistry in table DR1; see also Anczkiewicz et al., 2007). No compositional difference is observed between MI-bearing and MI-free garnets.

## SUPPLEMENTARY METHODS

*GASP geobarometer:* Holdaway (2001) and Koziol and Newton (1988). Anorthite activity for the GASP barometer was obtained from the bulk composition of the mesoperthite in garnet (similar method used in Carswell & O´Brien, 1993), while grossular activity in garnet was calculated using the activity models from Berman and Aranovich (1996).
*Ternary feldspar thermometer:* Fuhrman & Lindsey (1988) on mesoperthite in garnet.

*Piston Cylinder re-homogenization experiments:* 30 garnet chips with crack-free, unexposed nanogranites were separated from at least 20 garnet crystals extracted from three different double-polished thick sections, and used as starting material. Since all the nanogranites investigated in the sample show the same phase assemblage, the nanogranites in the selected chips can be considered a representative population of the investigated inclusions.
Experiments were performed by using Pt-capsules of 4mm length, 3mm diameter, and cold sealed after filling with the garnet chips and quartz. Each run lasted 24/48 hours (Table DR2). The Pt-capsule was placed in a talc-pyrex-graphite-pressure cell. The inner part of the assemblage, embedding the Pt-capsule, consists of crushable alumina ($Al_2O_3$). Type S thermocouple (Pt/PtRh10) was used to control the temperature in the experiments and its uncertainty was assumed to be +/- 10 °C. Pressure was calibrated using the quartz-coesite transition and accuracy was estimated to be +/- 0.05 GPa. Each experiment was performed without adding water (Frei et al 2009) as previous works showed no compositional difference between microcrack-free nanogranites re-homogenized under dry or wet conditions (Bartoli et al. 2013). Quenching of the experimental charge was performed at high pressure, unloading

the machine only when ambient T was reached. Experimental charges have been then mounted in epoxy and polished to expose re-homogenized inclusions (further details on benefits and limits of this approach in Bartoli et al., 2013).

*FESEM and microprobe:* Microstructural investigation and EDS elemental mapping were undertaken using the field-emission microprobe JEOL Hyperprobe JXA-8500F available in the Museum für Naturkunde in Berlin.
Glasses and mineral phases have been analyzed using the microprobe JEOL JXA-8200 available at the Institut für Erd- und Umweltwissenschaften of University of Potsdam. 15 KV, 3.5 nA and variable beam diameter depending on the inclusions size (1µm or 3 µm) have been used as analytical parameters for glass analyses, after calibration using $H_2O$-bearing leucogranitic glass standards. Alkali-loss is generally expected during analyses of alkali-rich melts (Morgan and London, 2005). The correction factors for Na, K, Si, Al has been estimated by analyzing leucogranitic standards of similar composition (6wt% $H_2O$, also used in Morgan and London, 2005) during each analytical session, with the same analytical conditions used for glass analyses (a similar procedure was followed e.g. by Ferrero et al., 2012). Na loss, and the subsequent applied correction factor, is variable, from 20% relative (1 µm beam diameter) to <1% (3 µm beam diameter) depending on the single inclusion. ).
The FeO content of the analyzed MI is higher than the experimental melts reported in table DR3, possibly as result of compositional differences between the protolith investigated in our case study and the starting material of the published experiments.

*Raman investigation:* Raman analyses were performed on a HORIBA Jobin Yvon LabRAM HR 800 at the Institut für Erd- und Umweltwissenschaften of University of Potsdam. The instrument is equipped with a Peltier cooled multichannel CCD detector and coupled with an Olympus BX41 petrographic microscope. An air-cooled Nd:YAG laser was used for excitation (λ=532 nm, laser power on the sample was 2-3 mW) with a grating 300 lines/mm, slit width set to 100 µm and confocal hole to 200 µm.
The Raman hyperspectral map of the $H_2O$-rich glass consists of a grid (17 x 17=289 points) of equidistant points separated by 1µm, with spatial resolution 1µm x 1µm. All the spectra have been acquired using a 100x objective between 100 $cm^{-1}$ and 4000 $cm^{-1}$, integrating 3 repetition of 30 s, with spectral resolution of 10 $cm^{-1}$. A representative spectrum of the interstitial glass shown in the Raman map is visible in fig. DR2.
The $H_2O$ content of the re-homogenized nanogranites have been estimated following the method of Thomas (2000). The glass $H_2O$ content is known to have a linear relationship to the ratio of the integral intensities of two characteristic Raman bands of the glass, 3550 $cm^{-1}$ (OH) and 490 $cm^{-1}$ (see Fig. DR3A; Thomas, 2000). All the spectra were acquired using a 100x objective and collected between 100 $cm^{-1}$ and 4000 $cm^{-1}$, integrating 3 repetition of 100s, with spectral resolution of 10 $cm^{-1}$. Measurements on glass standards of rhyolitic composition with known $H_2O$ content provided a linear calibration curve (Fig. DR3B). This calibration was thus used to calculate the $H_2O$ content of 17 different MI in four garnet chips (Fig. DR3C). The integral intensities were estimated in the range 200-650 $cm^{-1}$ (glass band) and 2800-3850 $cm^{-1}$ ($H_2O$ band) both on standard glasses and re-homogenized inclusions after background correction / host subtraction.

| | | | | | In Nanogranites | | |
|---|---|---|---|---|---|---|---|
| | Grt | | Msp in Grt | Cpx | *Ep* | *Bt* | *Plag ($Pl_1$)* |
| wt% | 312 (core) | 289 (rim) | av2 | 12 | 254 | 14 | 21 |
| $Na_2O$ | 0,04 | 0,04 | 4,48 | 5,91 | 0,01 | 0,13 | 9,29 |
| MgO | 2,67 | 3,71 | 0,00 | 6,67 | 0,01 | 4,45 | 0,00 |
| $Al_2O_3$ | 21,47 | 21,32 | 19,94 | 10,05 | 23,86 | 18,24 | 23,69 |
| $SiO_2$ | 38,11 | 38,19 | 65,18 | 53,30 | 37,58 | 34,29 | 62,61 |
| $K_2O$ | 0,00 | 0,03 | 9,27 | 0,00 | 0,00 | 8,93 | 0,35 |
| CaO | 10,80 | 10,14 | 0,67 | 13,68 | 22,73 | 0,45 | 4,14 |
| $TiO_2$ | 0,16 | 0,13 | 0,01 | 0,52 | 0,21 | 0,37 | 0,03 |
| $Cr_2O_3$ | 0,00 | 0,04 | n.a. | 0,03 | n.a. | n.a. | n.a. |
| MnO | 0,48 | 0,37 | 0,01 | 0,07 | 0,10 | 0,20 | 0,01 |
| FeO | 26,22 | 25,34 | 0,25 | 10,17 | 13,87 | 30,09 | 0,71 |
| Total | 99,95 | 99,30 | 99,81 | 100,39 | 98,37 | 97,16 | 100,83 |
| | 12 (O) | 12 (O) | 8 (O) | 6 (O) | 12.5 (O) | 22 (O) | 8 (O) |
| Si | 3,002 | 3,010 | 2,943 | 1,935 | 3,056 | 5,401 | 2,761 |
| Ti | 0,010 | 0,007 | 0,000 | 0,014 | 0,013 | 0,044 | 0,001 |
| Al | 1,993 | 1,981 | 1,061 | 0,430 | 2,287 | 3,387 | 1,231 |
| Cr | 0,000 | 0,002 | 0,000 | 0,001 | 0,000 | 0,000 | 0,000 |
| $Fe^{3+}$ | 0,000 | 0,000 | 0,000 | 0,087 | 0,000 | 0,000 | 0,000 |
| $Fe^{2+}$ | 1,727 | 1,670 | 0,010 | 0,222 | 0,943 | 3,963 | 0,026 |
| Mn | 0,032 | 0,025 | 0,000 | 0,002 | 0,007 | 0,027 | 0,001 |
| Mg | 0,314 | 0,436 | 0,000 | 0,361 | 0,001 | 1,045 | 0,000 |
| Ca | 0,911 | 0,856 | 0,032 | 0,532 | 1,980 | 0,076 | 0,196 |
| Na | 0,005 | 0,006 | 0,392 | 0,416 | 0,001 | 0,041 | 0,794 |
| K | 0,000 | 0,003 | 0,562 | 0,000 | 0,000 | 1,795 | 0,020 |
| Alm/Ac | 58 | 56 | - | 11 | - | - | - |
| Pyp/Jd | 11 | 15 | - | 42 | - | - | - |
| Sps/Di | 1 | 1 | - | 46 | - | - | - |
| Grs | 31 | 29 | - | - | - | - | - |
| Ab % | - | - | 41 | - | - | - | 79 |
| An % | - | - | 4 | - | - | - | 19 |
| Or % | - | - | 55 | - | - | - | 2 |
| Mg# / Ps | 0,15 | - | - | - | 0,29 | 0,21 | - |

**Table DR1.** Mineral phase chemistry. Msp= mesoperthite; Ps=pistacite content in Epidote.

| EXPERIMENTAL PARAMETERS | | | | RESULTS | | | |
|---|---|---|---|---|---|---|---|
| Experiment Name | Temperature (°C) | Pressure (GPa) | Duration (h) | Re-melting | Decrepitation | Melt-host interaction | Complete re-homogenization |
| 1 | 950 | 2.0 | 24 | X | X (extensive) | - | - |
| 2 | 900 | 2.0 | 48 | X | X | X (new Grt) | - |
| 3 | 850 | 2.0 | 48 | - | - | - | - |
| 4 | 875 | 2.2 | 48 | X | X | X (new Grt) | - |
| 5 | 875 | 2.5 | 48 | X | X | X (limited) | - |
| 6 | 900 | 3.0 | 48 | X | X (extensive) | X (new Cpx) | X |
| **7 and 8** | **875** | **2.7** | **48** | **X** | **-** | **-** | **X** |

**Table DR2.** Re-homogenization experiments, with experimental parameters and relevant microstructural observations.

| | Re-homogenized nanogranites | | | | | | | | | | | | | | | | | | | Experimental Melts | | | | OSZ |
|---|---|---|---|---|---|---|---|---|---|---|---|---|---|---|---|---|---|---|---|---|---|---|---|---|
| name | 31 | 33 | 36* | 41 | 42 | 5 | Mle8* | 27 | 3 | 75 | 77 | 80* | 81* | 3 | 4 | 6* | 28 | 2 | av. | std.dev. | A-06 | HS-08 | LIT-00 | TR-05 | Bulk |
| $SiO_2$ | 68,85 | 65,33 | 67,56 | 69,58 | 70,36 | 68,02 | 67,79 | 67,20 | 70,48 | 71,65 | 70,31 | 67,59 | 67,92 | 70,91 | 70,45 | 68,34 | 65,60 | 68,87 | 68,71 | 1,78 | 70,30 | 63,11 | 68,66 | 66,89 | 65,67 |
| $TiO_2$ | 0,12 | 0,06 | 0,06 | 0,25 | 0,16 | 0,00 | 0,09 | 0,06 | 0,33 | 0,04 | 0,13 | 0,18 | 0,09 | 0,15 | 0,05 | 0,03 | 0,09 | 0,00 | 0,10 | 0,09 | 0,17 | 0,27 | 0,24 | 0,23 | 0,68 |
| $Al_2O_3$ | 13,64 | 13,51 | 13,87 | 12,91 | 12,73 | 14,20 | 13,98 | 13,26 | 13,37 | 12,57 | 12,73 | 14,07 | 14,01 | 13,30 | 13,25 | 14,64 | 15,30 | 13,17 | 13,58 | 0,71 | 15,09 | 13,30 | 14,32 | 15,02 | 14,56 |
| FeO | 2,01 | 2,46 | 1,35 | 2,40 | 2,34 | 1,39 | 1,32 | 2,60 | 2,59 | 2,56 | 2,55 | 1,25 | 1,16 | 2,34 | 2,63 | 1,20 | 2,34 | 1,94 | 2,02 | 0,57 | 0,48 | 0,70 | 0,86 | 0,94 | 6,80 |
| MnO | 0,00 | 0,00 | 0,00 | 0,00 | 0,00 | 0,00 | 0,00 | 0,00 | 0,00 | 0,00 | 0,00 | 0,00 | 0,00 | 0,00 | 0,00 | 0,00 | 0,00 | 0,00 | 0,00 | 0,00 | 0,06 | 0,04 | 0,01 | 0,06 | 0,11 |
| MgO | 0,12 | 0,19 | 0,08 | 0,08 | 0,06 | 0,07 | 0,09 | 0,02 | 0,09 | 0,10 | 0,06 | 0,04 | 0,05 | 0,03 | 0,11 | 0,11 | 0,12 | 0,00 | 0,08 | 0,04 | 0,20 | 0,48 | 0,12 | 0,38 | 0,79 |
| CaO | 0,79 | 0,74 | 0,64 | 0,48 | 0,44 | 0,67 | 0,71 | 0,52 | 0,55 | 0,55 | 0,52 | 0,52 | 0,55 | 0,50 | 1,22 | 0,97 | 2,43 | 0,87 | 0,76 | 0,46 | 0,28 | 1,08 | 1,25 | 0,57 | 3,55 |
| $Na_2O$ | 3,76 | 5,55 | 4,38 | 4,24 | 3,77 | 4,26 | 5,21 | 5,19 | 4,43 | 3,98 | 4,01 | 4,50 | 4,15 | 4,39 | 4,11 | 4,69 | 2,19 | 3,49 | 4,24 | 0,74 | 4,98 | 4,42 | 4,01 | 4,08 | 3,43 |
| $K_2O$ | 4,15 | 4,66 | 4,36 | 4,23 | 4,28 | 4,37 | 4,74 | 4,79 | 4,50 | 4,37 | 4,48 | 4,94 | 4,93 | 4,23 | 4,64 | 3,56 | 5,68 | 4,16 | 4,50 | 0,44 | 4,43 | 3,52 | 4,67 | 5,20 | 2,53 |
| $P_2O_5$ | 0,05 | 0,00 | 0,05 | 0,00 | 0,03 | 0,00 | 0,00 | 0,00 | 0,00 | 0,06 | 0,07 | 0,00 | 0,10 | 0,04 | 0,00 | 0,03 | 0,00 | 0,00 | 0,02 | 0,03 | 0,00 | 0,17 | 0,00 | 0,00 | 0,24 |
| TOTAL | 93,48 | 92,50 | 92,34 | 94,16 | 94,16 | 92,98 | 93,92 | 93,63 | 96,33 | 95,87 | 94,85 | 93,08 | 92,94 | 95,90 | 96,46 | 93,57 | 93,76 | 92,49 | 94,02 | 1,34 | 95,99 | 87,10 | 94,15 | 93,37 | 98,36 |
| Q | 28 | 14 | 23 | 26 | 29 | 24 | 17 | 17 | 24 | 29 | 27 | 20 | 23 | 26 | 24 | 24 | 24 | 29 | 24 | 4 | 23 | 28 | 26 | 21 | 23 |
| C | 2 | 0 | 1 | 0 | 1 | 1 | 0 | 0 | 0 | 0 | 1 | 0 | 1 | 1 | 0 | 1 | 1 | 1 | 0 | 1 | 2 | 5 | 0 | 2 | 0 |
| Or | 25 | 28 | 26 | 25 | 25 | 26 | 28 | 28 | 27 | 26 | 26 | 29 | 29 | 25 | 27 | 21 | 34 | 25 | 27 | 3 | 26 | 30 | 29 | 31 | 15 |
| Ab | 32 | 44 | 37 | 36 | 32 | 36 | 44 | 42 | 38 | 34 | 34 | 38 | 35 | 37 | 35 | 40 | 19 | 29 | 36 | 6 | 42 | 32 | 36 | 35 | 29 |
| An | 4 | 0 | 3 | 2 | 2 | 3 | 1 | 0 | 3 | 2 | 2 | 3 | 2 | 2 | 4 | 5 | 12 | 4 | 4 | 3 | 1 | 2 | 7 | 3 | 16 |
| Hy | 4 | 3 | 3 | 4 | 4 | 3 | 1 | 4 | 4 | 5 | 5 | 2 | 2 | 4 | 4 | 2 | 4 | 4 | 4 | 1 | 1 | 2 | 2 | 2 | 14 |
| ASI | 1,13 | 0,87 | 1,06 | 1,04 | 1,09 | 1,10 | 0,93 | 0,90 | 1,02 | 1,02 | 1,03 | 1,03 | 1,06 | 1,05 | 0,95 | 1,10 | 1,08 | 1,11 | 1,03 | 0,07 | 1,12 | 1,02 | 1,03 | 1,12 | 0,98 |
| $H_2O$ by diff | 6,52 | 7,50 | 7,66 | 5,84 | 5,84 | 7,02 | 6,08 | 6,37 | 3,67 | 4,13 | 5,15 | 6,92 | 7,06 | 4,10 | 3,54 | 6,43 | 6,24 | 7,51 | 5,97 | 1,34 | 3.06** | 10.00** | 5,85 | 6,63 | 0,44*** |
| Mg# | 0,10 | 0,12 | 0,09 | 0,06 | 0,04 | 0,08 | 0,11 | 0,01 | 0,06 | 0,07 | 0,04 | 0,05 | 0,07 | 0,02 | 0,07 | 0,14 | 0,08 | 0,00 | 0,06 | 0,04 | 0,40 | 0,53 | 0,20 | 0,40 | 0,17 |
| $K_2O/Na_2O$ | 1,10 | 0,84 | 0,99 | 1,00 | 1,13 | 1,03 | 0,91 | 0,92 | 1,02 | 1,10 | 1,12 | 1,10 | 1,19 | 0,96 | 1,13 | 0,76 | 2,59 | 1,19 | 1,06 | 0,39 | 0,89 | 0,80 | 1,16 | 1,27 | 0,74 |
| $K_2O/H_2O$ | 0,64 | 0,62 | 0,57 | 0,72 | 0,73 | 0,62 | 0,78 | 0,75 | 1,23 | 1,06 | 0,87 | 0,71 | 0,70 | 1,03 | 1,31 | 0,55 | 0,91 | 0,55 | 0,75 | 0,23 | 1,45 | 0,35 | 0,80 | 0,78 | 1,54 |

**Table DR3.** Dataset of re-homogenized nanogranites EMP analyses (from four different garnet chips) and compositions of high and ultra-high pressure melts (see also caption Fig.4A). Analyses marked with * are re-homogenized nanogranites containing euhedral quartz. The $H_2O$ content as provided by the authors (indicated with **) has been reintegrated in the reported compositions to allow a direct comparison with the EMP analyses of re-homogenized inclusions. OSZ: Orlica-Śnieżnik leucogranulites bulk chemistry. ***=LOI. ASI: Alumina Saturation Index (molar $Al_2O_3/CaO+Na_2O+K_2O$). Mg#= molar MgO/(MgO+FeO). Experimental melts are referred as follow: **AU-06** = Auzanneau et al., (2006), **HS-08** = Hermann and Spandler (2008), **LIT-00** = Litvinovsky et al., (2000), **TR-05** = Tropper et al. (2005).

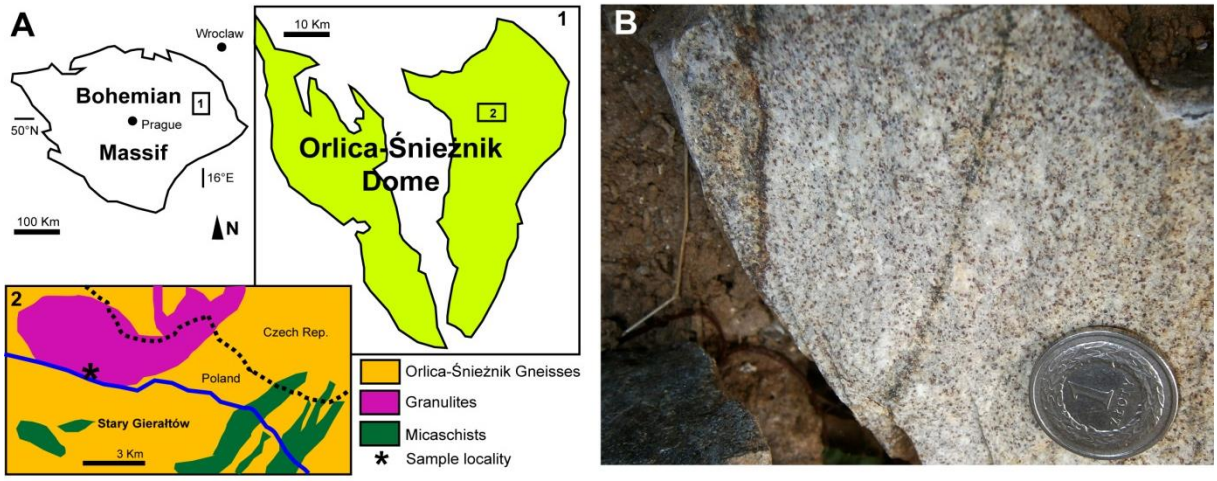


**Fig. DR1.** A) Schematic geological setting of the Orlica-Śnieżnik Dome (modified after Anczkiewicz et al, 2007) and its location in the Bohemian Massif. 1: Orlica-Śnieżnik Dome. 2: Location of the Granulite body. *Star:* sampling locality; B) Hand sample of leucogranulites collected along the Biała Lądecka river.

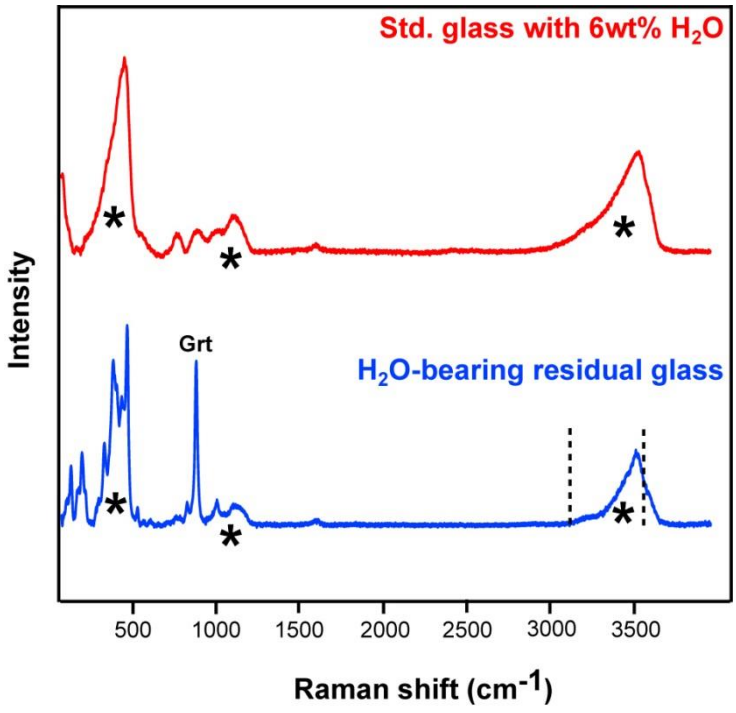


**Fig. DR2.** Representative Raman spectra of interstitial $H_2O$-rich glass in nanogranites before re-homogenization (*blue*) with secondary signals from other phases in the inclusion, and $H_2O$-bearing standard glass (*red*; Morgan & London, 2005) after background correction. *=characteristic Raman bands of glass. *Black dashed lines*= spectral region reported in Raman map of Fig. 3.

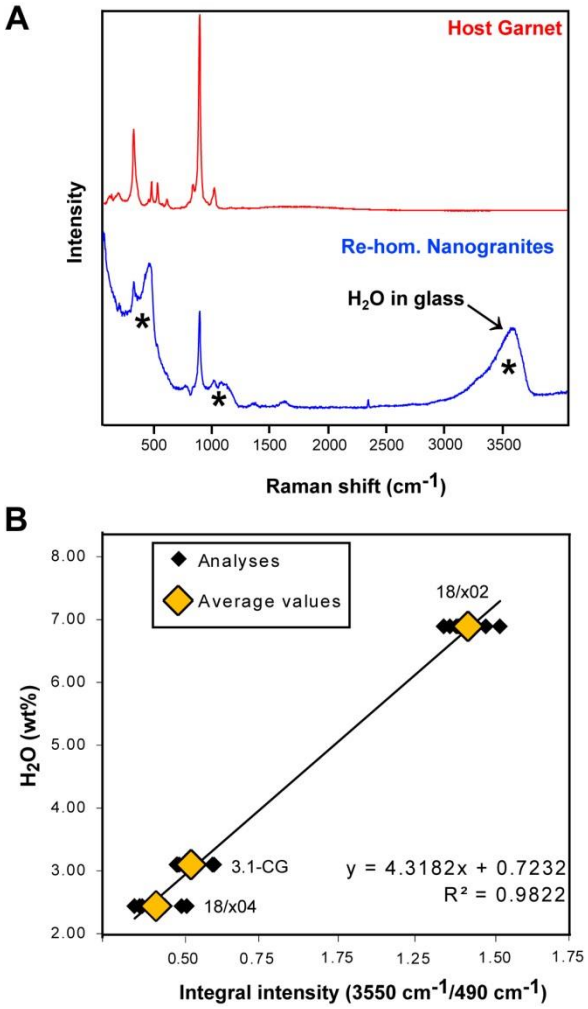


C

| Name | Intensity (3550 cm$^{-1}$ /490 cm$^{-1}$) | $H_2O$ |
|---|---|---|
| MI 1 | 0,98 | 4,96 |
| MI 3 | 1,37 | 6,62 |
| MI 4-73 | 1,22 | 6,00 |
| MI 4crack | 1,04 | 5,20 |
| MI 5 | 1,04 | 5,22 |
| MI 7c | 1,54 | 7,38 |
| MI 8-1 | 1,86 | 8,75 |
| MI 8-711 | 1,62 | 7,73 |
| MI 9b | 1,56 | 7,46 |
| MI 11a | 1,78 | 8,41 |
| MI 12 | 0,92 | 4,69 |
| MI 12 | 1,10 | 5,48 |
| MI 12b | 0,95 | 4,81 |
| MI 14 | 1,31 | 6,37 |
| MI 15 b | 1,81 | 8,55 |
| MI 16 | 1,22 | 5,97 |
| MI 17 | 1,74 | 8,24 |
| Average | 1,36 | 6,59 |
| Std.dev. | 0,33 | 1,43 |

**Fig. DR3.** A) Raman spectra of re-homogenized nanogranites (*blue*) without background correction, and host garnet (*red*). The bands characteristic of a granitic glass are indicated with *. Host garnet main peaks, residual carbon coating (1250-1750 cm-1) and atmospheric $N_2$ (2331 cm$^{-1}$) are visible as minor signals. B) Calibration curve for the estimate of $H_2O$ content of silicatic glasses. *18/x04 and 18/x02*= rhyolitic glasses with $H_2O$ content 2.44 and 6.89 wt % respectively, synthesized and characterized using infrared spectroscopy and Karl Fischer titration by Almeev et al. (2012); *3.1-CG*= leucogranite with 3.1 wt % $H_2O$ (Morgan and London, 2005). C) Results of $H_2O$ calculations on re-homogenized nanogranites.

## *REFERENCES*


Almeev, R., Bolte, T., Nash, B., Holtz, F., Erdmann, M., Cathey, H. (2012), High temperature, low $H_2O$ silicic magmas of the Yellowstone hotspot: an experimental study of rhyolite from the Bruneau-Jarbidge eruptive center: Journal of Petrology, v. 53, p. 1837-1866, doi: 10.1093/petrology/egs035.

Anczkiewicz, R., Szczepański, J., Mazur, S., Storey, C., Crowley, Q., Villa, I.M., Thirlwall, M.F., and Jeffries, T.E., 2007, Lu-Hf geochronology and trace element distribution in garnet: Implications for uplift and Exhumation of ultra-high pressure granulites in the Sudetes, SW Poland: Lithos, v. 95, p. 363–380, DOI: 10.1016/j.lithos.2006.09.001.

Bakun-Czubarow, N., 1991, Quartz pseudomorphos after coesite and quartz exoutions in eclogitic omphacites of the Złote Mountains in the Sudetes, SW Poland: Archiwum Mineralogiczne, v. 48, p. 3–25.

Bartoli, O., Cesare, B., Poli, S., Acosta-Vigil, A., Esposito, R., Turina, A., Bodnar, R.J., Angel, R.J., and Hunter, J., 2013, Nanogranite inclusions in migmatitic garnet: behavior during piston cylinder re-melting experiments: Geofluids, v. 13, p. 405–420, DOI: 10.1111/gfl.12038.

Berman, R.G., and Aranovich, L.Y., 1996, Optimized standard state and solution properties of minerals. I. Model calibration for olivine, orthopyroxene, cordierite, garnet, and ilmenite in the system FeO-MgOCaO-$Al_2O_3$-$TiO_2$-$SiO_2$: Contributions to Mineralogy and Petrology, v. 126, p. 1–4.

Bröcker, M., Klemd, R., Cosca, M., Brock, W., Larionov, A.N., and Rodionov, N., 2009, The timing of eclogite facies metamorphism and migmatization in the Orlica-Śnieżnik complex, Bohemian Massif: constraints from a multimethod geochronological study: Journal of Metamorphic Geology, v. 27, p. 385–403.

Carswell, D. A., and O'Brien, P. J., 1993. Thermobarometry and geotectonic significances of high-pressure granulites: examples from the Moldanubian Zone of the Bohemian Massif in Lower Austria. Journal of Petrology, 34, 427–459.

Don, J., Dumicz, M., Wojciechowska, I. and Żelaźniewicz, A., 1990, Lithology and tectonics of the Orlica–Śnieżnik Dome, Sudetes; recent state of knowledge: Neues Jahrbuch für Geologie und Paläontologie, v. 179, p. 159–188.

Ferrero, S., Bartoli, O., Cesare, B., Salvioli-Mariani, E., Acosta-Vigil, A., Cavallo, A., Groppo, C., and Battiston, S., 2012, Microstructures of melt inclusions in anatectic metasedimentary rocks: Journal of Metamorphic Geology, v. 30, p. 303–322, DOI: 10.1111/j.1525-1314.2011.00968.x.

Frei, D., Liebscher, A., Franz, G., Wunder, B., Klemme, S., and Blundy, Jon, 2009, Trace element partitioning between orthopyroxene and anhydrous silicate melt on the lherzolite solidus from 1.1 to 3.2 GPa and 1,230 to 1,530°C in the model system $Na_2O$-CaO-MgO-$Al_2O_3$-$SiO_2$: Contributions to Mineralogy and Petrology, v. 157, p. 473-490, DOI 10.1007/s00410-008-0346-5.

Fuhrman, M.L., and Lindsley, D.H., 1988, Ternary feldspar modeling and thermometry: American Mineralogist, v. 73, p. 201–215.

Gordon, S.M., Schneider, D.A., Manecki, M., and Holm, D.K., 2005, Exhumation and metamorphism of an ultrahigh-grade terrane : geochronometric investigations of Sudete Mountains (Bohemia), Poland and Czech Republic: Journal of the Geological Society of London, v. 162, p. 841–855.

Holdaway, M.J., 2001, Recalibration of the GASP geobarometer in light of recent garnet and plagioclase activity models and versions of the garnet-biotite geothermometer: American Mineralogist, v. 86, p. 1117–1129.

Koziol, A., and Newton, R., 1988, Redetermination of the anorthite breakdown reaction and improvement of the plagioclase-garnet-$Al_2SiO_5$-quartz geobarometer: American Mineralogist, V. 73, p. 216–223.

Kröner, A., Jaeckel, P., Hegner, E., and Opletal, M., 2001, Single zircon ages and whole-rock Nd isotopic systematics of early Palaeozoic granitoid gneisses from the Czech and Polish Sudetes (Jizerské hory, Krkonoše and Orlica–Snežnik Complex): International Journal of Earth Sciences (Geol. Rundschau), v. 90, p. 304–324.

Kryza, R., Pin, C., and Vielzeuf, D., 1996, High pressure granulites from the Sudetes (SW Poland): evidence of crustal subduction and collisional thickening in the Variscan Belt: Journal of Metamorphic Geology, v. 14, p. 531–546, DOI: 10.1046/j.1525-1314.1996.03710.x.

Lange, U., Bröcker, M., Armstrong, R., Trapp, E., and Mezger, K., 2005, Sm–Nd and U–Pb dating of high-pressure granulites from the Złote and Rychleby Mts (Bohemian Massif, Poland and Czech Republic): Journal of Metamorphic Geology, v. 23, p. 133–145 DOI: 10.1111/j.1525-1314.2005.00566.x.

Morgan VI, G.B., and London, D., 2005, Effect of current density on the electron microprobe analysis of alkali aluminosilicate glasses: American Mineralogist, v. 90, p. 1131–1138.

Oliver, G.J.H., Corfu, F., and Krogh, T.E., 1993, U–Pb ages from SW Poland: evidence for a Caledonian suture zone between Baltica and Gondwana: Journal of the Geological Society, London, v. 150, p. 355–369.

Štípská, P., Schulmann, K., and Kröner, A., 2004, Vertical extrusion and middle crustal spreading of omphacite granulite: a model of syn-convergent exhumation (Bohemian Massif, Czech Republic): Journal of Metamorphic Geology, v. 22, p. 179–198.

Thomas, R., 2000, Determination of water contents of granite melt inclusions by confocal laser Raman microprobe spectroscopy: American Mineralogist, v. 85, p. 868–872.

Turniak, K., Mazur, S. and Wysoczański, R., 2000, SHRIMP zircon geochronology and geochemistry of the Orlica–Śnieżnik gneisses (Variscan belt of Central Europe) and their tectonic implications: Geodinamica Acta, v. 13, p. 1–20.